ACS PHYSICAL CHEMISTRY Au
AN OPEN ACCESS JOURNAL OF THE AMERICAN CHEMICAL SOCIETY

pubs.acs.org/physchemau
Article

Molecular Insights into Cu/Zn Metal Response to the Amyloid β-Peptide (1−42)

Anurag Prakash Sunda* and Anuj Kumar Sharma*

Cite This: ACS Phys. Chem Au 2024, 4, 57−66
Read Online

ACCESS | Metrics & More | Article Recommendations | Supporting Information

ABSTRACT: Aβ1−40 peptide and Aβ1−42 peptide are the building units of beta-amyloid plaques present in Alzheimer's disease (AD)-affected brain. The binding affinity of various divalent metal ions such as Cu and Zn present in AD-affected brain with different amino acids available in Aβ-peptide became the focus to explore their role in soluble neurotoxic oligomer formation. Cu^{2+} metal ions are known to enhance the neurotoxicity of the Aβ1−42 peptide by catalyzing the formation of soluble neurotoxic oligomers. The competitive preference of both Cu^{2+} and Zn^{2+} simultaneously to interact with the Aβ-peptide is unknown. The divalent Cu and Zn ions were inserted in explicit aqueous Aβ1−42 peptide configurations to get insights into the binding competence of these metal ions with peptides using classical molecular dynamics (MD) simulations. The metal-ion interactions reveal that competitive binding preferences of various peptide sites become metal-ion-specific and differ significantly. For Cu^{2+}, interactions are found to be more significant with respect to those of Asp-7, His-6, Glu-11, and His-14. Asp-1, Glu-3, Asp-7, His-6, Glu-11, and His-13 amino acid residues show higher affinity toward Zn^{2+} ions. MD simulations show notable variation in the solvent-accessible surface area in the hydrophobic region of the peptide. Infinitesimal mobility was obtained for Zn^{2+} compared to Cu^{2+} in an aqueous solution and Cu^{2+} diffusivity deviated significantly at different time scales, proving its labile features in aqueous Aβ1−42 peptides.

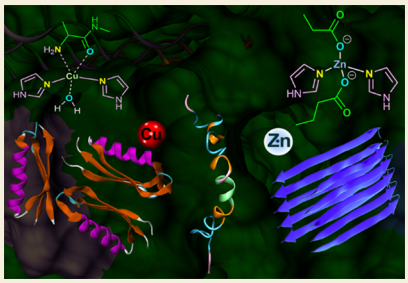

KEYWORDS: *molecular dynamics, amyloid β-peptide, residue mean distance map, radial distribution function, solvent accessible surface area*

1. INTRODUCTION

Within the diagnostic capability of various neurodegenerative diseases, enormous efforts have been made over the years to inquest Alzheimer's disease (AD) in the human brain.[1−7] The well-known fact of AD proposed pathologies is the deposition of beta amyloid plaques which are the aggregates of 40 or 42 long amino acid chains, i.e., Aβ1−40 peptide or Aβ1−42 peptides, respectively (comparatively more involvement of Aβ1−42 peptide).[4,8−10] In the past three decades, various aspects of Alzheimer's disease-affected brain have been put forward such as the concentration of metal ions,[10−14] formation of Aβ aggregates,[15−18] amyloid toxicity,[1,19−21] impact of chelators,[7,8,15] hydrophobicity of amino-acid chain residues, etc.[7,22] Moreover, the influence of factors such as pH,[23] temperature, and buffer have also been noticed in the deposition of Aβ aggregates.[21] In the past decade, theoretical investigations of several structural features of aggregates have made significant advancements in our understanding of Aβ-fibrils.[5,10,23−47] Post-mortem examination of the brain suggested that bioavailable metals (i.e., copper, zinc, and iron) are found in high concentrations in the amyloid plaques as compared to the surrounding tissues.[6] Naturally, immense interest in understanding the role of metal ions has emerged in the scientific community. A detailed investigation has been carried out to probe their coordination with different amino acids available in Aβ peptides.[5,15,16,22,48] Interestingly, it has been observed that while all these metal ions in different oxidation states coordinate with Aβ peptides, experimental studies have distinguished Cu^{2+} and Zn^{2+} ions in amyloid-β peptide aggregation and found that the Cu^{2+} ions lead to the stabilizing of soluble neurotoxic oligomers compared to larger Aβ1−42 peptide nontoxic aggregates in the presence of Zn^{2+} ions.[7,16,20,21,49] Among transition metal ions, the coordination chemistry of Cu and Zn with amyloid-β peptide has been widely explored in the last two decades.[2,16,20,21,49−56] There are several divergent reports on the coordinating amino acid residues of the Aβ1−42 peptide that form the coordination sphere of the metal ions. The binding of different amino acids to metal ions seems to depend on various experimental conditions such as pH, buffer medium, temperature, etc.[7,20,21,51] Drew et al.[57−61] have explored in detail the role of metal ions in redox activity with the amyloid-β peptide and the binding affinity of Cu^{2+} ions with the peptide. Although the binding pockets of the Aβ1−42 peptide have been identified

Received: August 11, 2023
Revised: October 3, 2023
Accepted: October 4, 2023
Published: October 25, 2023

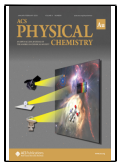

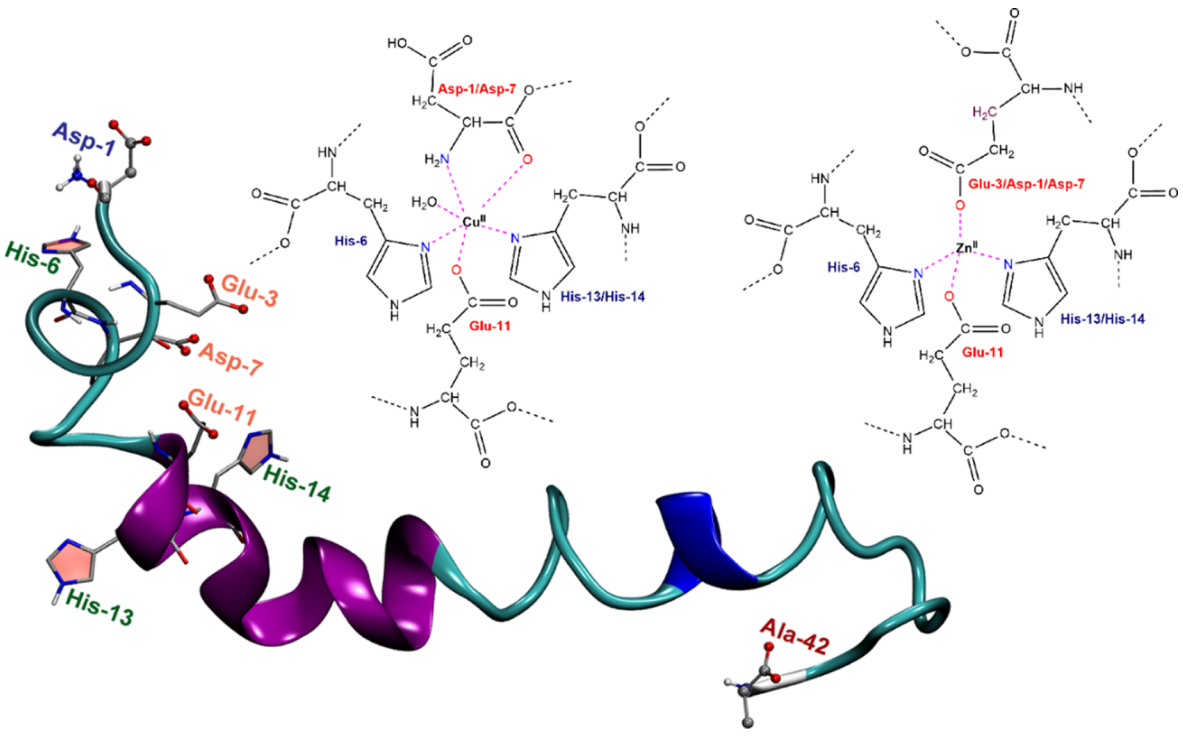

Figure 1. Energy-minimized structure of the Aβ1−42 peptide with various metal binding amino acids/sites. Color scheme for the secondary structure: coil—white, turn—cyan, α-helix—purple, 3-helix—blue. The metal binding sites are shown with a dashed bond (magenta color) for Cu^{2+} and Zn^{2+} along with coordinating N atoms (blue) and the O atom (red) of amino acids.

for such metal ions, the important aspect of catalyzing such specific aggregations in the presence of both Cu^{2+} and Zn^{2+} ions *simultaneously* is still unknown. Prabhakar and co-workers[62] elucidated the mechanism of dimerization of the Aβ1−42 peptide using MD simulations and found the effective role of the hydrophobic region within the two monomers involved in the dimerization process. Khatua et al.[63] determined conformational changes in the Aβ1−42 peptide and the response of the surrounding solvent with respect to the aggregation process. The authors provided key insights from their atomistic simulations of entropy variation along with conformational transitions in the Aβ1−42 peptide. Recently, Man et al.[64] examined the effect of various force fields using replica exchange MD on the secondary structure of the Aβ1−42 peptide dimer. The authors concluded that dimer stabilization occurs due to nonspecific interactions irrespective of conformational differences arising in secondary structure from a specific force field.

Boopathi and Kolandaivel[48] performed MD simulations to probe the role of metal ions in Aβ1−40 peptide and Aβ1−42 peptide aggregation by comparing with their Cu^{2+} configuration and Zn^{2+} configurations, respectively. The authors predicted significant changes in the secondary structures of the Aβ1−40 peptide and the Aβ1−42 peptide in the presence of either Cu^{2+} or Zn^{2+} ions. Coskuner and Perry's group[25,27,42,47,65] demonstrated the use of computational methods to unveil several structural characteristics and thermodynamic aspects of metal-bound Aβ-peptides. In the present study, we have considered the Aβ1−42 peptide as an AD amyloid precursor and inserted both Cu and Zn divalent ions in the same configuration with the same concentration (4 Cu^{2+}: 4 Zn^{2+}) to analyze the competitive preference of these metals ions in the explicit aqueous phase of the Aβ1−42 peptide using classical molecular dynamics (MD) simulations. The binding sites for both Zn^{2+} and Cu^{2+} ions reported in experiment studies[22] at various pH include **N**-atom and **O**-atom of Asp-1, Glu-3, His-6, Asp-7, Glu-11, His-13, and His-14, as depicted in Figure 1. This study focuses on characterizing binding affinities of metal ions to these peptide sites in the concurrent presence of Cu^{2+} and Zn^{2+} ions through MD simulations and analyzing the relative strengths. The setup of the system configuration and computational details of MD simulations are provided in the next section.

2. COMPUTATIONAL METHODS

Classical all-atom simulations were carried out on the hydrated Aβ1−42 peptide using the molecular dynamics package GROMACS 4.5.4.[66] The initial structure of the Aβ1−42 peptide was obtained from a previous study[67] (PDB: 1IYT) on the 42 long-amino-acid Aβ1−42 peptide. An energy-minimized monomer configuration (Figure 1) from the steepest descent method was used to generate 16 chain configurations of the Aβ1−42 peptide for better statistical averages. It was further solvated with 10,000 spc/e[68] water molecules (as per the cubic simulation box size, i.e., 72.9 Å) to generate an explicit water environment around the peptides, and Na^+/Cl^- ions were added. We have used the spc/e water model instead of Tip4p to get better dynamics of metal ions in the aqueous phase, which may be affected by water dynamics significantly. As the diffusion coefficient of water in the spc/e water model is in close agreement with the experimental value, we opted for the spc/e water model. The NPT ensemble was used initially for avoiding any free volume around peptides or ions and 1 ns canonical ensemble (NVT) pre-equilibration was carried out at 310 K using the velocity-rescale thermostat.[69] The particle-mesh Ewald method[70,71] was used to model long-range interactions, and nonbonded interactions were truncated at 11 Å. All bonded or nonbonded potential parameters for the Aβ1−42 peptide and metal ion interactions were taken from the GROMOS force field 53A6.[72] In order to assess the impact of Cu and Zn divalent ions, *four* Zn/Cu ions each were added in pre-equilibrated configuration by maintaining charge neutrality (by adding Cl^- ions) in 1:4 ratio with respect to the amyloid peptide (4 Cu^{2+}: 4 Zn^{2+}: 16 Aβ1−42 chains) and to get optimum statistical averages of the peptide structure and dynamics of ions. Further, 1 ns equilibration was carried

https://doi.org/10.1021/acsphyschemau.3c00041
ACS Phys. Chem Au 2024, 4, 57−66

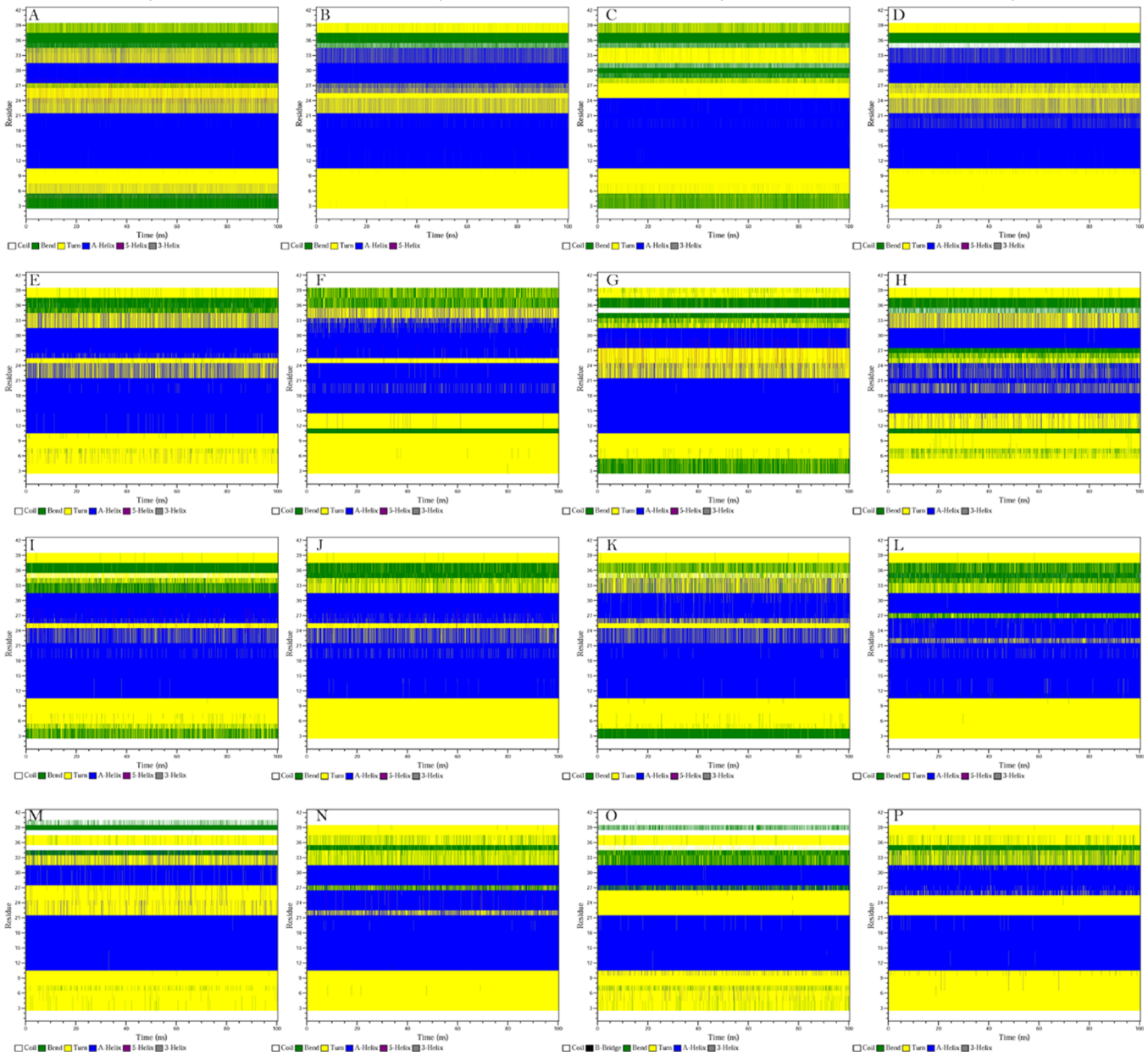

Figure 2. Secondary structure variation in Aβ1−42 peptide chains [A-P] for 1 to 42 (on the *y*-axis) amino-acid segments as a function of simulation time (1 to 100 ns on the *x*-axis). Color scheme for coil—white, bend—green, turn—yellow, α-helix—blue, 5-helix—brown, 3-helix—gray (for more clarity of each figure, please see Figure S1a−d in the Supporting Information).

out using the NVT ensemble, and the cubic simulation box size is 73.70 Å. A 100 ns production run was performed at 310 K using an isothermal−isobaric ensemble (NPT) with a time step of 1 fs, thermostat coupling of 0.3 ps, reference pressure of 1 bar with pressure coupling of 1 ps, and compressibility of 4.5×10^{-5} bar^{-1}. The pressure was maintained using a Parrinello−Rahman barostat and temperature was regulated using a Nosé−Hoover[73,74] thermostat. The secondary structure of all the 16 Aβ1−42 peptide chains was analyzed using the DSSP protocol.[75]

3. RESULTS AND DISCUSSION

3.1. Secondary Structure of Peptides

A microscopic view is essential to understand the conformational signatures of the Aβ1−42 peptide in the presence of transition metal ions and an explicit aqueous environment. The secondary structure formation and its suppression at different peptide regions are important for amyloid aggregation.

We have calculated secondary structure variation in each Aβ1−42 peptide chain (A-P) as a function of simulation time. Figure 2 shows the secondary structure behavior of various Aβ1−42 peptide chains obtained from a 100 ns simulation trajectory. In most of the Aβ1−42 peptide chains, the peptide regions 3−10 show a turn, and 9−21 show an α-helix structure. The peptide regions 21 to 31 largely fluctuate between turn and helical conformation.

For different chains, the peptide regions 3−5 and 31−40 show interchange in bend or turn conformations. Our results predict 38−42% helical structure in Aβ1−42 peptide chains in the presence of metal ions, which is 10% higher than the simulation results obtained by Boopathi and Kolandaivel.[48] The observations in the present study closely resemble the finding of

https://doi.org/10.1021/acsphyschemau.3c00041
ACS Phys. Chem Au 2024, 4, 57−66

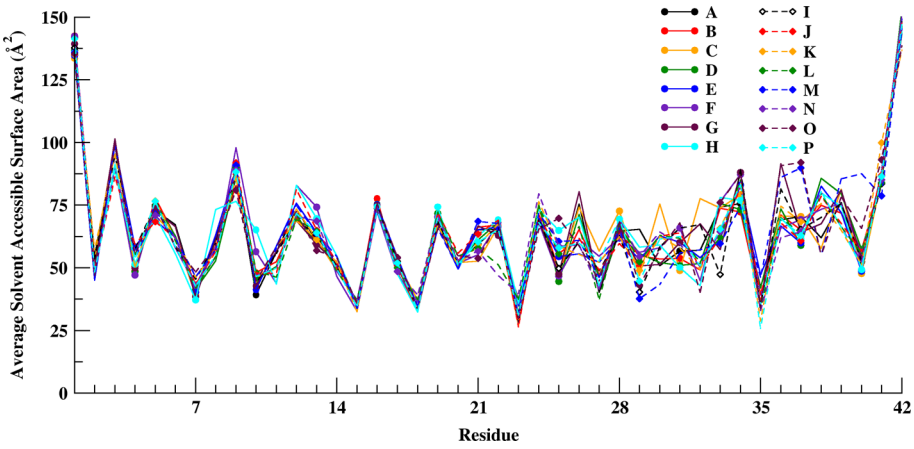

Figure 3. Variation in the average SASA of the Aβ1−42 peptide as a function of peptide chain residues 1−42.

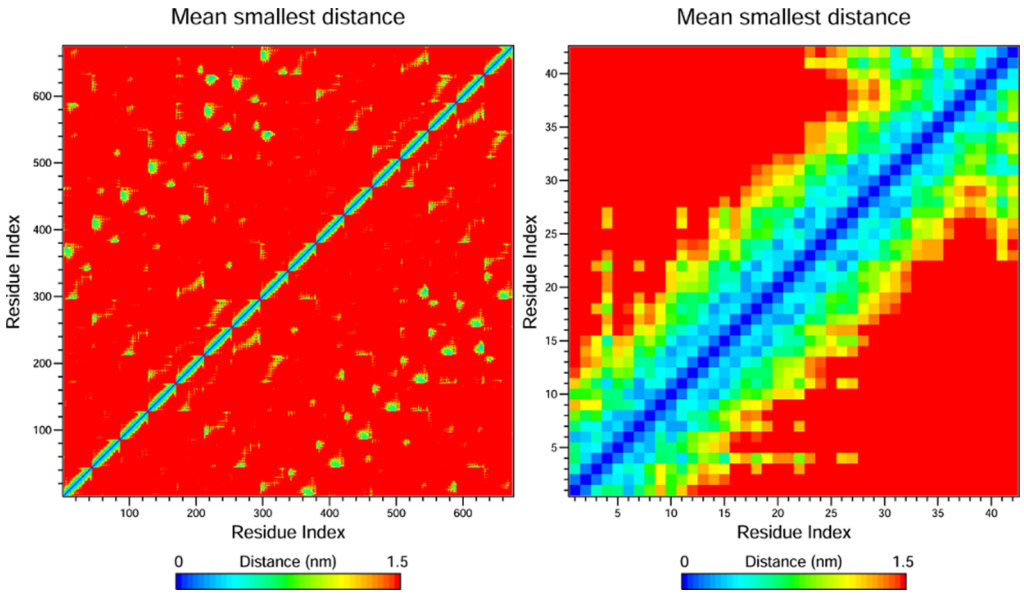

Figure 4. Mean smallest distance calculated from 100 ns NPT simulation run (left) for all residues (16 chains) and (right) for a randomly chosen single chain of the Aβ1−42 peptide.

Coskuner[42] toward more abundant helical and turn structure conformation. Among 16 peptide chain configurations, the first 10 amino acid residues show coil followed by a turn helical pattern for the peptide chains B, D, J, L, N, and P. However, there is an interchange between the bend or turn structure for the peptide chains A, C, G, I, K, and O, specifically for the 3−5 peptide residue sequence. Except for the peptide chains F and H, there is a consistent pattern of the α-helix structure for the 11−21 peptide chain region.

The structural changes in peptide chains are characterized by calculating the average solvent accessible surface area of the Aβ1−42 peptide as a function of peptide chain residues 1 to 42. Figure 3 shows that the average solvent accessible surface area (SASA) for the first 1−20 chain residues of all the 16 chains "A" to "P" almost overlap and have the same signatures. A key fluctuation in the average SASA value is observed among various Aβ1−42 peptide chains for the chain residues 21 to 42. It shows that a significant variation takes place on their surface sites and in interchain peptide interactions for the chain residue 21 to 42 (out of that 30−42 is largely known as hydrophobic[65]). Apart from metal ions, It reflects that the hydrophobic peptide part equally participates in the preaggregation of Aβ1−42 peptide chains.

A similar observation has been illustrated by Khatua et al.[63] by examining conformational disorderedness and solvent heterogeneity around the peptide segments. Figure 4 shows the protein contact map calculated as the mean smallest distance of amino acid residue pairs of the Aβ1−42 peptide within the cutoff distance of 1.5 nm. The similarities in the contact map matrix for all 16 chains (Figure 4a) can be seen above and below the diagonal. The contact map observed in one chain is depicted for a randomly chosen peptide, as shown in Figure 4b).

3.2. Influence of Cu^{2+} and Zn^{2+} Metal Ions

3.2.1. Metal−Residue Interactions. In order to evaluate the binding site affinity of both the Cu^{2+} and Zn^{2+} metal ions, the radial distribution functions (RDFs) are calculated for different peptide chain residues with respect to their center of mass around the metal ions. Figure 5a shows an RDF profile for interactions of Zn2+ ions with the center of mass of Asp-1, Glu-3, His-6, Asp-7, Glu-11, and His-13/His-14 chain residues. The high peak intensity at 3.9 Å for Asp-1 peptide chain residue interactions with Zn^{2+} shows a strong metal binding affinity with

https://doi.org/10.1021/acsphyschemau.3c00041
ACS Phys. Chem Au 2024, 4, 57−66

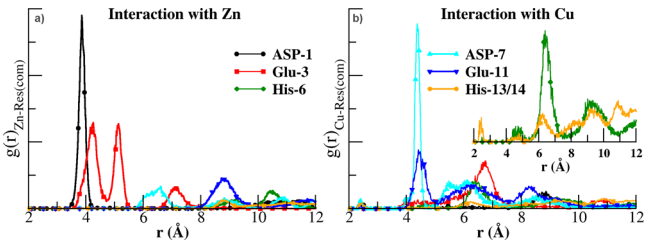

Figure 5. Radial distribution functions calculated from 100 ns NPT simulation for the (a) Zn^{2+} metal ion and (b) Cu^{2+} metal ions, respectively (metal ions and between the center of mass of peptide chain residues such as Asp-1, Glu-3, Asp-7, His-6, Glu-11, His-13, and His-14, respectively) (the inset depicts His-6/13/14 peptide residue interactions with Cu^{2+} ions).

Asp-1. A comparatively low and bifurcated intense peak (4.1 and 5 Å distance) is obtained for Glu-3. The equal distribution of intensity for both arms of the bifurcated peak indicates the possible binding of Zn^{2+} ions with two different chains which leads to the assembling of two chains in the form of dimer. However, the peak intensity of RDFs for Zn^{2+} toward the His-6 and His-13/His-14 peptide chain residues are comparatively insignificant in the measured time scale due to the competitive affinity of Cu^{2+} ions simultaneously.

Similar to the Zn^{2+} ions RDF profile, the interactions of Cu^{2+} ions with peptide chain residues are shown in Figure 5b. Unlike Zn^{2+} ions, the interactions of His-6/His-14 are found to be more prominent with Cu^{2+} ions rather than for Asp-1 and Glu-3 peptide chain residues. These observations are in agreement with earlier MD simulations of Jiao and Yang[76] where histidine N atoms act as the anchor coordinating sites for Cu^{2+} binding. However, peptide Cu^{2+} ion interactions with Asp-1 are well reported in earlier ab initio studies where metal ions are placed around the preferential coordinating sites of the oligomer.[65,77,78] In the case of Cu^{2+} ions, most significant interactions are seen for Asp-7 and Glu-11 peptide chain residues at 4.1 Å. The peak intensity is much higher for Asp-7 compared to Glu-11. The inset of Figure 5b differentiates Cu^{2+} interactions with His-6 and His-14 peptide chain residues. Santis et al.[79] demonstrated through the X-ray study that the simultaneous addition of both Cu^{2+} and Zn^{2+} ions resulted in partial binding of both metal ions with peptide and differed in binding to various histidine residues. These metal interactions with the center of mass of peptide residues are further examined through specific atomic sites.

3.2.2. Metal-Binding Atomic Site Interactions with Peptide Chain Residues. As depicted in Figure 1, RDFs are calculated from the 100 ns trajectory to evaluate binding affinities toward the preferential atomic binding sites of metal ions[22] with Asp-1/Asp-7, His-6/His-13/His-14, and Glu-3/Glu-11 using N atoms and O atoms. Figure 6a–c shows RDFs for Cu^{2+} metal ions with an N atom of His-6/His-13/His-14/Asp-1 and an O atom of Asp-1/Asp-7/Glu-3/Glu-11 amino acid residues. The RDF of the Cu–N atom of the His-14 residue shows much stronger interactions at a shorter distance (~5 Å) compared to the Cu–N atom of the His-6 residue (~7 Å) (see Figure 6a). These interactions with His-13 residue are found to be insignificant. The interactions of Cu^{2+} ions are not observed with Asp-1 amino acid residue either with the N atom or with the O atom (see Figure 6b). The Cu–O atom RDFs for Asp-7, Glu-3, and Glu-11 illustrate that the Cu^{2+} ion shows significant interactions with the O atom of Asp-7 and Glu-11 peptide residue at 3 Å. The coordination number (CN) contribution of these atomic interactions is calculated around the Cu^{2+} ions in the first solvation shell (Table 1). The CN is observed at 0.14 to 0.20 for the N atoms/O atoms of the Asp-7, His-6, Glu-11, and

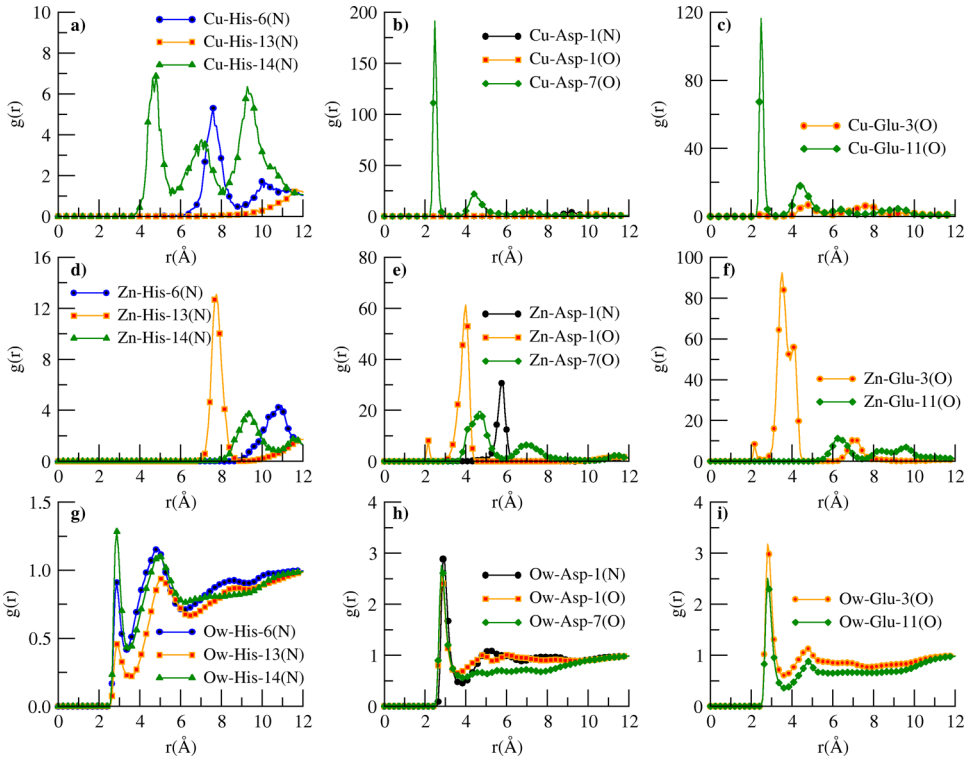

Figure 6. RDFs calculated from the 100 ns trajectory for the peptide chain interactions of N atoms and O atoms of Asp-1, Glu-3, Asp-7, His-6, Glu-11, His-13, and His-14 amino acids with the (a–c) Cu^{2+} ion, (d–f) Zn^{2+} ion, and (g–I) oxygen atom of water molecules, respectively.

https://doi.org/10.1021/acsphyschemau.3c00041
ACS Phys. Chem Au 2024, 4, 57–66

Table 1. Coordination Number (CN) Calculated from the 100 ns Trajectory for the Cu^{2+}, Zn^{2+} Ion, and Oxygen Atom (O_w) of Water Molecules with Respect to the N-Atom and the O-Atom of Amino Acids, Respectively (the Distance Cutoff for the Solvation Shell Is Shown in Parentheses)

amino acid residue	atom of amino acid residue	CN with respect to Cu^{2+} ions	CN with respect to Zn^{2+} ions	CN with respect to O_w atoms of water molecules
Asp-1	N		0.24 (6.2 Å)	0.006 (3.6 Å)
Asp-1	O		0.25 (4.5 Å)	0.006 (3.6 Å)
Asp-7	O	0.14 (3 Å)	0.24 (6.0 Å)	0.006 (3.6 Å)
His-6	N	0.15 (9 Å)	0.21 (9.9 Å)	0.003 (3.6 Å)
His-13	N		0.24 (8.5 Å)	0.002 (3.6 Å)
His-14	N	0.20 (8 Å)	0.18 (10 Å)	0.003 (3.6 Å)
Glu-3	O	0.01 (3 Å)	0.50 (5.0 Å)	0.007 (3.6 Å)
Glu-11	O	0.16 (3 Å)	0.29 (8.0 Å)	0.006 (3.6 Å)

His-14 peptide chain residues, which show comparatively significant metal−peptide interactions.

Similar to Cu^{2+} ions, RDFs are calculated for Zn^{2+} ions with the N atom of His-6/His-13/His-14/Asp-1 and the O atom of Asp-1/Asp-7/Glu-3/Glu-11 amino acid residues (see Figure 6d−f). The Zn − N atom RDF profiles of His-6/His-13/His-14 in Figure 6d depict that interactions of the Zn^{2+} ion with the N atom of the histidine residue occur at a much larger distance (above 7 Å) compared to Cu^{2+} ions. Moreover, the Zn^{2+} ions show stronger interactions with the Asp-1 peptide residue, as seen in Figure 6e. For Asp-1, An intense peak is observed at ∼5.8 Å for the Zn−N atom RDF and at ∼4 Å for the Zn−O atom RDF, respectively. These Zn−O atom interaction peaks are obtained at a slightly higher distance at 4.7 Å for Asp-7. The comparison of the Zn−O atom RDF peak for Glu-3 and Glu-11 peptide residue illustrates that interactions of Glu-3 residue are more significant. The CN for Zn^{2+} metal ion is found to be in the range of 0.21−0.29 for Asp-1, Asp-7, His-6, Glu-11, and His-13 (Table 1) except 0.5 for Glu-3 and 0.18 for His-14. The Zn^{2+} ions show relatively higher affinity for the N atom as well as O atom sites of Asp-1, Glu-3, Asp-7, His-6, Glu-11, His-13, and His-14 amino acid residues of peptides. In previous simulation studies,[42,48] the emphasis on Zn^{2+} ion−peptide residue interaction is limited to Asp-7 and Glu-11 while the interactions of Asp-1 and Glu-3 are equally significant.

3.2.3. Water−Peptide Residue Interactions. To demonstrate the role of water in the metal ion−peptide structure, the RDF of the Ow atom of water molecules is calculated from the 100 ns trajectories to differentiate the water solvation properties around the preferential binding sites of Asp-1, Glu-3, Asp-7, His-6, Glu-11, His-13, and His-14 amino acid residues of peptides. Figure 6g−i depicts interactions of the O_w atom of water molecules with the N atom of His-6/His-13/His-14/Asp-1 and the O atoms of Asp-1/Asp-7/Glu-3/Glu-11 amino acid residues. The RDF between O_w and N atom of His-6/His-13 shows a less intense peak at 2.9 Å and CN is also found to be 0.002−0.003. The interactions of water with Asp-1, Glu-3, Asp-7, and Glu-11 show an intense RDF peak at 2.9 Å, as seen in Figure 6h, i. The CN of water molecules around these residues at the first solvation shell (3.6 Å) is found to be 0.006. This suggests that the N atom environment of His-6 and His-13 residues relatively exhibits poor hydrogen bonding with water molecules compared to that of Asp-1/Asp-7 and Glu-3 and Glu-11 amino acid residues of the peptide. For metal ions, the calculated CN of water molecules at the first solvation shell (3.6 Å) is 5 and 6 for Cu^{2+} and Zn^{2+} ions, respectively.

3.3. Metal Influence on Interchain Residue Interactions

The interaction of metal ions with different binding sites of the Aβ1−42 peptide which spread over more than one chain residue leads to significant variation in their sequential arrangement. In the absence of metal ions, Figure 7a, b depicts an array of Aβ1−42 peptide chains such as 2−4−4−4−2 obtained from NVT equilibration. This array can be visualized as a top view (Figure 7a) and a side view (Figure 7b). It clearly shows that the initial configuration is well separated in equal and remains superimposed (top-down or feed-forward manner).

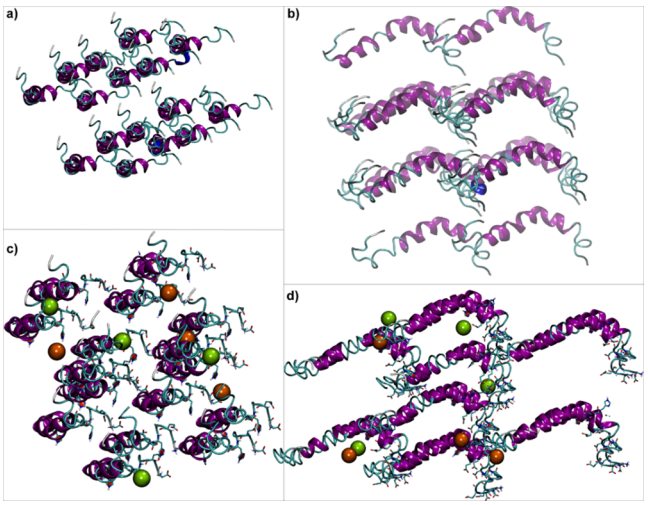

Figure 7. Snapshot of Aβ1−42 peptide chains [A to P] (a and b) without metal ions from NVT pre-equilibration; (c and d) entangled Aβ1−42 peptide chains [A to P] in a sequential pattern at 80 ns NPT production run assisted by metal ions, respectively. Color scheme for the secondary structure (new cartoon): coil—white, turn—cyan, α-helix—purple, 3-helix—blue, residues 1, 3, 6, 7, 11, 13, and 14 are shown as surface, Cu^{2+} ions: green, and Zn^{2+} ions—orange.

After the insertion of metal ions, these peptide chain arrays realigned themselves along with binding enforcement caused by metal ions. Figure 7c shows a top view, and (d) Figure 7d shows a side view obtained randomly after an 80 ns NPT production simulation run. The important observation that can be seen from these snapshots is that the top-down arrangements get rearranged completely in a 4−8−4 sequential pattern (side view) where the tail of two Aβ1−42 peptides interacts with the head of four Aβ1−42 peptide chains, assisted by metal ions. It can be visualized easily from the top-side view, as shown in Figure 8. Such sequential patterns can be visualized in all residue-contact maps (Figure 4).

3.4. Mobility of Metal Ions

To examine the dynamics in metal ions around the peptide chains in explicit water, mean square displacement (MSD) is plotted against simulation time using the Einstein relationship.[80] The MSDs are calculated in each 25 ns time segment such as I, II, III, and IV of a total 100 ns trajectory obtained from NPT simulations. These MSD plots were found to be straight lines for Cu^{2+}, Na^{+}, and Cl^{-} ions and water molecules (see Figure S2 for the Supporting Information). MSD plots were found to be nonlinear with an increase in simulation time for Zn^{2+} ions (see Figure S2 for the Supporting Information). It clearly indicates that Zn^{2+} ions get immobilized around the peptide chains due to their strong affinity toward amino acid residues of the peptides. Compared to Zn^{2+} ions, the mean square displacement shows a

https://doi.org/10.1021/acsphyschemau.3c00041
ACS Phys. Chem Au 2024, 4, 57−66

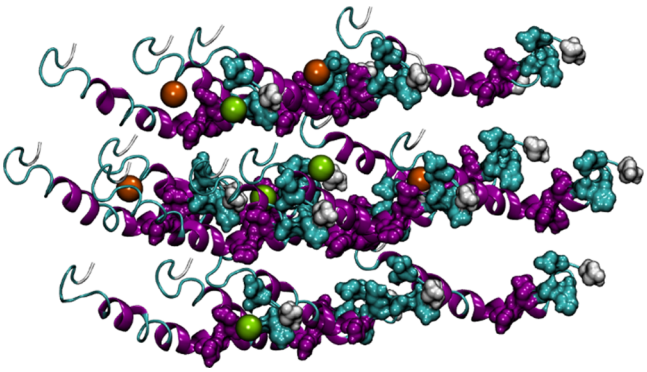

Figure 8. Snapshot of entangled Aβ1−42 peptide chains [A-P] in the sequential pattern at 80 ns assisted by metal ions. Color scheme for the secondary structure (new cartoon): coil—white, turn—cyan, α-helix—purple, 3-helix—blue, residues 1, 3, 6, 7, 11, 13, and 14 are shown as surface, Cu^{2+} ions—green, and Zn^{2+} ions—orange.

linear increase with the simulation time for all four segments. Similar observations are seen for Na^+ and Cl^- ions. The slope of the MSD plot, i.e., diffusion coefficient (D) is obtained from 2 to 22 ns linear regime and is provided in Table 2.

The water diffusion coefficients obtained for all four segments are similar and are in good agreement with diffusion coefficients of bulk spc/e water (i.e., 2.6×10^{-5} cm^2 s^{-1}).[68] In the case of Cl^- ions, the diffusion coefficients show a deviation of 0.1 in each segment from the average value of all four segments. A similar trend is seen in the case of the Na^+ ions. The diffusivity of Na^+ ions is found to be reduced by a factor of 0.6 compared to that of Cl^- ions. The diffusivity of Cu^{2+} is found to be lowered by a factor of 6.7 compared to the Na^+ ions and lowered by a factor of 11 compared to the Cl^- ions. The lower value of the diffusion coefficient for Cu^{2+} ions than Na^+ ions could be due to the size of the cation. Moreover, there is a large deviation of 0.1 in each segment, which is quite significant for Cu^{2+} mobility. It is important to note that the indifferent mobility of Cu^{2+} ions in each segment compared to immobilized Zn^{2+} ions suggests that Cu^{2+} ions have a labile nature and do not get trapped in local binding sites of amino acids like Zn^{2+} ions within the observed simulation time scale.

4. CONCLUSIONS

In summary, an attempt has been made using MD simulations to get molecular insights on competitive binding of divalent Cu and Zn ion interactions with the Aβ1−42 peptide. The metal ion interactions reveal that competitive binding preferences of various peptide sites such as ASP-1, Glu-3, His-6, Asp-7, Glu-11, and His13/14 become metal-ion-specific and differ significantly for both metal ions. An unevenly low mobility of Cu^{2+} ions compared to immobilized Zn^{2+} ions trapped in local binding sites of amino acids suggests that Cu^{2+} ions have a highly labile nature within the observed simulation time scale around the Aβ1−42 peptide. It indicates a competitive preference for the Zn^{2+} ions over the Cu^{2+} ions. Since metal ions are known to coordinate with the Aβ1−42 peptide and it is expected to affect their aggregation, the present work can be envisaged to provide some insight into the observations in prior studies that Cu and Zn affect the aggregation of the Aβ1−42 peptide differently, and Cu especially leads to the stabilization of soluble neurotoxic oligomers. Cu^{2+} ions show preferential binding affinity toward the N atoms/O atoms of the Asp-7, His-6, Glu-11, and His-14 peptide chain residues. The binding affinity of Zn^{2+} ions is comparatively more significant than that of Cu^{2+} ions and floats over N atoms/O atoms of the Asp-1, Glu-3, Asp-7, His-6, Glu-11, His-13, and His-14 amino acid residues of the peptide. The comparison of dual metal ion affinity unveils that Cu^{2+} metal ions toward His-13 is almost negligible, which has a limited view through single ion model simulations or experiments. Moreover, the previous studies placed more emphasis on the confirmation variation of the β-sheet structure of the Aβ1−42 peptide. The present simulations suggest that in addition to structural variations in the presence of dual ions the metal-peptide and peptide-water interactions of preferential atomic binding sites play an equally crucial role.

To conclude, the response of metal ions with Aβ1−42 peptide as competitive interactions of Zn^{2+} ions over the Cu^{2+} ions requires due consideration for future QM/MM studies to examine metal ion impact simultaneously where metal ions are placed as per their preferential locations around the oligomers. The labile nature of Cu^{2+} ions observed in the present work compared to Zn^{2+} ions essentially needs due attention in the presence of metal ions such as Fe, Al, etc., and simulations as a function of pH[81] for longer time-scale are under progress.

■ ASSOCIATED CONTENT

Supporting Information

The Supporting Information is available free of charge at https://pubs.acs.org/doi/10.1021/acsphyschemau.3c00041.

Enlarged Figure 2. MSD plots for metal ions calculated from MD simulations (PDF)

■ AUTHOR INFORMATION

Corresponding Authors

Anurag Prakash Sunda − *Department of Chemistry, J. C. Bose University of Science and Technology, YMCA, Faridabad 121006, India;* orcid.org/0000-0001-9186-1970; Email: anurag@jcboseust.ac.in, anurag.sunda@gmail.com

Anuj Kumar Sharma − *Department of Chemistry, School of Chemical Sciences and Pharmacy, Central University of Rajasthan, Ajmer 305817, India;* orcid.org/0000-0002-5090-3713; Email: anuj.sharma@curaj.ac.in, aks.iitk@gmail.com

Complete contact information is available at: https://pubs.acs.org/10.1021/acsphyschemau.3c00041

Table 2. Diffusion Coefficient ($D \times 10^{-5}$ cm^2/s) Calculated in Each 25 ns Time Interval of 100 ns Trajectory For Cu^{2+}, Na^+, Cl^- Ions, and Water Molecules, Respectively

time segment	simulation time (ns)	Cu^{2+} ions	Na^+ ions	Cl^- ions	water
I	0−25	0.0394 (±0.1070)	0.6549 (±0.0054)	1.1716 (±0.2439)	2.6277 (±0.0360)
II	25−50	0.2407 (±0.0070)	0.7825 (±0.0086)	0.9339 (±0.0512)	2.6389 (±0.0083)
III	50−75	0.0169 (±0.0297)	0.5878 (±0.0036)	1.0484 (±0.0326)	2.6134 (±0.0100)
IV	75−100	0.0716 (±0.0104)	0.4212 (±0.0810)	0.9609 (±0.0652)	2.6208 (±0.0585)

https://doi.org/10.1021/acsphyschemau.3c00041
ACS Phys. Chem Au 2024, 4, 57−66

Author Contributions

The manuscript was written through the equal contributions of the authors. CRediT: **Anurag Prakash Sunda** conceptualization, data curation, formal analysis, funding acquisition, investigation, methodology, software, validation, visualization, writing-original draft, writing-review & editing; **Anuj Kumar Sharma** conceptualization, formal analysis, funding acquisition, writing-original draft, writing-review & editing.

Funding

CRG/2022/001938 & CRG/2022/004355; [F. 30−589/2021 (BSR)]

Notes

The authors declare no competing financial interest.

■ ACKNOWLEDGMENTS

A.P.S. acknowledges the "University Grants Commission" for research grants under the Basic Scientific Research scheme [F. 30-589/2021 (BSR)]. A.P.S. and A.K.S. acknowledge the Science and Engineering Research Board (SERB), New Delhi, for CRG/2022/001938 and CRG/2022/004355 Grants, respectively.

■ REFERENCES

(1) Hardy, J.; Higgins, G. Alzheimer's disease: the amyloid cascade hypothesis. *Science* **1992**, *256*, 184−185.
(2) Bush, A.; Pettingell, W.; Multhaup, G. D.; Paradis, M.; Vonsattel, J.; Gusella, J.; Beyreuther, K.; Masters, C.; Tanzi, R. Rapid induction of Alzheimer A β amyloid formation by zinc. *Science* **1994**, *265*, 1464−1467.
(3) Gaggelli, E.; Kozlowski, H.; Valensin, D.; Valensin, G. Copper Homeostasis and Neurodegenerative Disorders (Alzheimer's, Prion, and Parkinson's Diseases and Amyotrophic Lateral Sclerosis). *Chem. Rev.* **2006**, *106*, 1995−2044.
(4) Rauk, A. The chemistry of Alzheimer's disease. *Chem. Soc. Rev.* **2009**, *38*, 2698−2715.
(5) Nasica-Labouze, J.; et al. Amyloid β Protein and Alzheimer's Disease: When Computer Simulations Complement Experimental Studies. *Chem. Rev.* **2015**, *115*, 3518−3563.
(6) Rajendran, R.; Minqin, R.; Ynsa, M. D.; Casadesus, G.; Smith, M. A.; Perry, G.; Halliwell, B.; Watt, F. A novel approach to the identification and quantitative elemental analysis of amyloid deposits—Insights into the pathology of Alzheimer's disease. *Biochem. Biophys. Res. Commun.* **2009**, *382*, 91−95.
(7) Savelieff, M. G.; Nam, G.; Kang, J.; Lee, H. J.; Lee, M.; Lim, M. H. Development of Multifunctional Molecules as Potential Therapeutic Candidates for Alzheimer's Disease, Parkinson's Disease, and Amyotrophic Lateral Sclerosis in the Last Decade. *Chem. Rev.* **2019**, *119*, 1221−1322.
(8) Sharma, A. K.; Pavlova, S. T.; Kim, J.; Finkelstein, D.; Hawco, N. J.; Rath, N. P.; Kim, J.; Mirica, L. M. Bifunctional Compounds for Controlling Metal-Mediated Aggregation of the Aβ42 Peptide. *J. Am. Chem. Soc.* **2012**, *134*, 6625−6636.
(9) Ridgley, D. M.; Barone, J. R. Evolution of the Amyloid Fiber over Multiple Length Scales. *ACS Nano* **2013**, *7*, 1006−1015.
(10) Pan, L.; Patterson, J. C. Molecular Dynamics Study of Zn(Aβ) and Zn(Aβ42). *PLoS One* **2013**, *8*, No. e70681.
(11) Lovell, M. A.; Robertson, J. D.; Teesdale, W. J.; Campbell, J. L.; Markesbery, W. R. Copper, iron and zinc in Alzheimer's disease senile plaques. *J. Neurol. Sci.* **1998**, *158*, 47−52.
(12) Scott, L. E.; Orvig, C. Medicinal Inorganic Chemistry Approaches to Passivation and Removal of Aberrant Metal Ions in Disease. *Chem. Rev.* **2009**, *109*, 4885−4910.
(13) Bush, A. I. The metallobiology of Alzheimer's disease. *Trends Neurosci.* **2003**, *26*, 207−214.
(14) Hamley, I. W. The Amyloid β Peptide: A Chemist's Perspective: Role in Alzheimer's and Fibrillization. *Chem. Rev.* **2012**, *112*, 5147−5192.
(15) Faller, P.; Hureau, C. Bioinorganic chemistry of copper and zinc ions coordinated to amyloid-β peptide. *Dalton Trans.* **2009**, 1080−1094.
(16) Faller, P. Copper and Zinc Binding to Amyloid-β: Coordination, Dynamics, Aggregation Reactivity and Metal-Ion Transfer. *Chembiochem* **2009**, *10*, 2837−2845.
(17) Zhang, Y.; Rempel, D. L.; Zhang, J.; Sharma, A. K.; Mirica, L. M.; Gross, M. L. Pulsed hydrogen-deuterium exchange mass spectrometry probes conformational changes in amyloid (Aβ) peptide aggregation. *Proc. Natl. Acad. Sci. U. S. A.* **2013**, *110*, 14604−14609.
(18) Ruggeri, F. S.; Adamcik, J.; Jeong, J. S.; Lashuel, H. A.; Mezzenga, R.; Dietler, G. Influence of the β-Sheet Content on the Mechanical Properties of Aggregates during Amyloid Fibrillization. *Angew. Chem., Int. Ed.* **2015**, *54*, 2462−2466.
(19) Hardy, J.; Selkoe, D. J. The Amyloid Hypothesis of Alzheimer's Disease: Progress and Problems on the Road to Therapeutics. *Science* **2002**, *297*, 353−356.
(20) Hureau, C.; Dorlet, P. Coordination of redox active metal ions to the amyloid precursor protein and to amyloid-β peptides involved in Alzheimer disease. Part 2: Dependence of Cu(II) binding sites with Aβ sequences. *Coord. Chem. Rev.* **2012**, *256*, 2175−2187.
(21) Sharma, A. K.; Pavlova, S. T.; Kim, J.; Kimb, J.; Mirica, L. M. The effect of Cu2+ and Zn2+ on the Aβ42 peptide aggregation and cellular toxicity. *Metallomics* **2013**, *5*, 1529−1536.
(22) Rana, M.; Sharma, A. K. Cu and Zn interactions with Aβ peptides: consequence of coordination on aggregation and formation of neurotoxic soluble Aβ oligomers. *Metallomics* **2019**, *11*, 64−84.
(23) Li, Y.; Xu, W.; Mu, Y.; Zhang, J. Z. H. Acidic pH retards the fibrillization of human islet amyloid polypeptide due to electrostatic repulsion of histidines. *J. Chem. Phys.* **2013**, *139*, No. 055102.
(24) Straub, J. E.; Thirumalai, D. Toward a Molecular Theory of Early and Late Events in Monomer to Amyloid Fibril Formation. *Annu. Rev. Phys. Chem.* **2011**, *62*, 437−463.
(25) Wise-Scira, O.; Xu, L.; Kitahara, T.; Perry, G.; Coskuner, O. Amyloid-β peptide structure in aqueous solution varies with fragment size. *J. Chem. Phys.* **2011**, *135*, 205101.
(26) Nguyen, P. H.; Li, M. S.; Derreumaux, P. Effects of all-atom force fields on amyloid oligomerization: replica exchange molecular dynamics simulations of the Aβ dimer and trimer. *Phys. Chem. Chem. Phys.* **2011**, *13*, 9778−9788.
(27) Wise-Scira, O.; Xu, L.; Perry, G.; Coskuner, O. Structures and free energy landscapes of aqueous zinc(II)-bound amyloidβ(1−40) and zinc(II)-bound amyloid-β(1−42) with dynamics. *J. Biol. Inorg. Chem.* **2012**, *17*, 927−938.
(28) Riccardi, L.; Nguyen, P. H.; Stock, G. Construction of the Free Energy Landscape of Peptide Aggregation from Molecular Dynamics Simulations. *J. Chem. Theory Comput.* **2012**, *8*, 1471−1479.
(29) Nguyen, P. H.; Derreumaux, P. Conformational Ensemble and Polymorphism of the All-Atom Alzheimer's Aβ42 Amyloid Peptide Oligomers. *J. Phys. Chem. B* **2013**, *117*, 5831−5840.
(30) Lemkul, J. A.; Bevan, D. R. Aggregation of Alzheimer's Amyloid β-Peptide in Biological Membranes: A Molecular Dynamics Study. *Biochemistry (Mosc.)* **2013**, *52*, 4971−4980.
(31) Xu, L.; Wang, X.; Wang, X. Effects of Zn2+ Binding on the Structural and Dynamic Properties of Amyloid β Peptide Associated with Alzheimer's Disease: Asp1 or Glu11? *ACS Chem. Neurosci.* **2013**, *4*, 1458−1468.
(32) Rosenman, D. J.; Connors, C. R.; Chen, W.; Wang, C.; García, A. E. Aβ Monomers Transiently Sample Oligomer and Fibril-Like Configurations: Ensemble Characterization Using a Combined MD/NMR Approach. *J. Mol. Biol.* **2013**, *425*, 3338−3359.
(33) Nguyen, P. H.; Li, M. S.; Derreumaux, P. Amyloid oligomer structure characterization from simulations: A general method. *J. Chem. Phys.* **2014**, *140*, No. 094105.
(34) Wise, O.; Coskuner, O. New force field parameters for metalloproteins: Divalent copper ion centers including three histidine

https://doi.org/10.1021/acsphyschemau.3c00041
ACS Phys. Chem Au 2024, 4, 57−66

residues and an oxygen-ligated amino acid residue. *J. Comput. Chem.* **2014**, *35*, 1278−1289.
(35) Smith, M. D.; Rao, J. S.; Segelken, E.; Cruz, L. Force-Field Induced Bias in the Structure of Aβ21-β30: A Comparison of OPLS, AMBER, CHARMM, and GROMOS Force Fields. *J. Chem. Inf. Model.* **2015**, *55*, 2587−2595.
(36) Liao, Q.; Kamerlin, S. C. L.; Strodel, B. Development and Application of a Nonbonded Cu2+ Model That Includes the Jahn−Teller Effect. *J. Phys. Chem. Lett.* **2015**, *6*, 2657−2662.
(37) Berhanu, W. M.; Alred, E. J.; Bernhardt, N. A.; Hansmann, U. H. All-atom Simulation of Amyloid Aggregates. *Phys. Procedia* **2015**, *68*, 61−68.
(38) Boopathi, S.; Kolandaivel, P. Study on the inter-and intra-peptide salt-bridge mechanism of Aβ23-β28 oligomer interaction with small molecules: QM/MM method. *Mol. BioSyst.* **2015**, *11*, 2031−2041.
(39) Boopathi, S.; Kolandaivel, P. Fe2+ binding on amyloid β-peptide promotes aggregation. *Proteins: Struct. Funct. Bioinf.* **2016**, *84*, 1257−1274.
(40) Brown, A. M.; Bevan, D. R. Molecular Dynamics Simulations of Amyloid β-Peptide (1−42): Tetramer Formation and Membrane Interactions. *Biophys. J.* **2016**, *111*, 937−949.
(41) Guisasola, E. E. B.; Gutiérrez, L. J.; Salcedo, R. E.; Garibotto, F. M.; Andujar, S. A.; Enriz, R. D.; Rodríguez, A. M. Conformational transition of Aβ42 inhibited by a mimetic peptide. A molecular modeling study using QM/MM calculations and QTAIM analysis. *Comput. Theor. Chem.* **2016**, *1080*, 56−65.
(42) Coskuner, O. Divalent copper ion bound amyloid-β(40) and amyloid-β(42) alloforms are less preferred than divalent zinc ion bound amyloid-β(40) and amyloid-β(42) alloforms. *J. Biol. Inorg. Chem.* **2016**, *21*, 957−973.
(43) Blinov, N.; Khorvash, M.; Wishart, D. S.; Cashman, N. R.; Kovalenko, A. Initial Structural Models of the Aβ42 Dimer from Replica Exchange Molecular Dynamics Simulations. *ACS Omega* **2017**, *2*, 7621−7636.
(44) Liao, Q.; Owen, M. C.; Bali, S.; Barz, B.; Strodel, B. Aβ under stress: the effects of acidosis, Cu^{2+}-binding, and oxidation on amyloid β-peptide dimers. *Chem. Commun.* **2018**, *54*, 7766−7769.
(45) Bhattacharya, S.; Xu, L.; Thompson, D. Revisiting the earliest signatures of amyloidogenesis: Roadmaps emerging from computational modeling and experiment. *WIREs Comput. Mol. Sci.* **2018**, *8*, No. e1359.
(46) Itoh, S. G.; Yagi-Utsumi, M.; Kato, K.; Okumura, H. Effects of a Hydrophilic/Hydrophobic Interface on Amyloid-β Peptides Studied by Molecular Dynamics Simulations and NMR Experiments. *J. Phys. Chem. B* **2019**, *123*, 160−169.
(47) Coskuner-Weber, O.; Uversky, V. N. Insights into the Molecular Mechanisms of Alzheimer's and Parkinson's Diseases with Molecular Simulations: Understanding the Roles of Artificial and Pathological Missense Mutations in Intrinsically Disordered Proteins Related to Pathology. *Int. J. Mol. Sci.* **2018**, *19*, 336.
(48) Boopathi, S.; Kolandaivel, P. Role of zinc and copper metal ions in amyloid β peptides Aβ(1̆40) and Aβ(1̆42) aggregation. *RSC Adv.* **2014**, *4*, 38951−38965.
(49) Zou, J.; Kajita, K.; Sugimoto, N. Cu2+ Inhibits the Aggregation of Amyloid β-Peptide(1−42) in vitro. *Angew. Chem., Int. Ed.* **2001**, *40*, 2274−2277.
(50) Huang, X.; Atwood, C. S.; Moir, R. D.; Hartshorn, M. A.; Vonsattel, J.-P.; Tanzi, R. E.; Bush, A. I. Zinc-induced Alzheimers Aβ1−40 Aggregation Is Mediated by Conformational Factors. *J. Biol. Chem.* **1997**, *272*, 26464−26470.
(51) Syme, C. D.; Nadal, R. C.; Rigby, S. E. J.; Viles, J. H. Copper Binding to the Amyloid-β (Aβ) Peptide Associated with Alzheimer's Disease: Folding, Coordination Geometry, pH Dependence, Stoichiometry, and Affinity of Aβ-(1−28): Insights From A Range of Complementary Spectroscopic Techniques. *J. Biol. Chem.* **2004**, *279*, 18169−18177.
(52) Mekmouche, Y.; Coppel, Y.; Hochgräfe, K.; Guilloreau, L.; Talmard, C.; Mazarguil, H.; Faller, P. Characterization of the ZnII Binding to the Peptide Amyloid-β1−16 linked to Alzheimer's Disease. *Chembiochem* **2005**, *6*, 1663−1671.
(53) Garai, K.; Sahoo, B.; Kaushalya, S. K.; Desai, R.; Maiti, S. Zinc Lowers Amyloid-β Toxicity by Selectively Precipitating Aggregation Intermediates. *Biochemistry* **2007**, *46*, 10655−10663.
(54) House, E.; Mold, M.; Collingwood, J.; Baldwin, A.; Goodwin, S.; Exley, C. Copper Abolishes the β-Sheet Secondary Structure of Preformed Amyloid Fibrils of Amyloid-β42. *J. Alzheimers Dis.* **2009**, *18*, 811−817.
(55) Eskici, G.; Axelsen, P. H. Copper and Oxidative Stress in the Pathogenesis of Alzheimer's Disease. *Biochemistry* **2012**, *51*, 6289−6311.
(56) Alies, B.; Solari, P.-L.; Hureau, C.; Faller, P. Dynamics of ZnII Binding as a Key Feature in the Formation of Amyloid Fibrils by Aβ11−28. *Inorg. Chem.* **2012**, *51*, 701−708.
(57) Drew, S. C.; Noble, C. J.; Masters, C. L.; Hanson, G. R.; Barnham, K. J. Pleomorphic Copper Coordination by Alzheimer's Disease Amyloid-β Peptide. *J. Am. Chem. Soc.* **2009**, *131*, 1195−1207.
(58) Mital, M.; Wezynfeld, N. E.; Fraczyk, T.; Wiloch, M. Z.; Wawrzyniak, U. E.; Bonna, A.; Tumpach, C.; Barnham, K. J.; Haigh, C. L.; Bal, W.; Drew, S. C. A Functional Role for Aβ in Metal Homeostasis? N-Truncation and High-Affinity Copper Binding. *Angew. Chem., Int. Ed.* **2015**, *54*, 10460−10464.
(59) Mital, M.; Zawisza, I. A.; Wiloch, M. Z.; Wawrzyniak, U. E.; Kenche, V.; Wróblewski, W.; Bal, W.; Drew, S. C. Copper Exchange and Redox Activity of a Prototypical 8-Hydroxyquinoline: Implications for Therapeutic Chelation. *Inorg. Chem.* **2016**, *55*, 7317−7319.
(60) Drew, S. C. The Case for Abandoning Therapeutic Chelation of Copper Ions in Alzheimer's Disease. *Front. Neurosci.* **2017**, *11*, 317.
(61) Mital, M.; Bal, W.; Frączyk, T.; Drew, S. C. Interplay between Copper, Neprilysin, and N-Truncation of β-Amyloid. *Inorg. Chem.* **2018**, *57*, 6193−6197.
(62) Zhu, X.; Bora, R. P.; Barman, A.; Singh, R.; Prabhakar, R. Dimerization of the Full-Length Alzheimer Amyloid β-Peptide (Aβ42) in Explicit Aqueous Solution: A Molecular Dynamics Study. *J. Phys. Chem. B* **2012**, *116*, 4405−4416.
(63) Khatua, P.; Jose, J. C.; Sengupta, N.; Bandyopadhyay, S. Conformational features of the Aβ-42 peptide monomer and its interaction with the surrounding solvent. *Phys. Chem. Chem. Phys.* **2016**, *18*, 30144−30159.
(64) Man, V. H.; Nguyen, P. H.; Derreumaux, P. High-Resolution Structures of the Amyloid-β 1−42 Dimers from the Comparison of Four Atomistic Force Fields. *J. Phys. Chem. B* **2017**, *121*, 5977−5987.
(65) Strodel, B.; Coskuner-Weber, O. Transition Metal Ion Interactions with Disordered Amyloid-β Peptides in the Pathogenesis of Alzheimer's Disease: Insights from Computational Chemistry Studies. *J. Chem. Inf. Model.* **2019**, *59*, 1782−1805.
(66) Hess, B.; Kutzner, C.; van der Spoel, D.; Lindahl, E. GROMACS 4: Algorithms for Highly Efficient, Load-Balanced, and Scalable Molecular Simulation. *J. Chem. Theory Comput.* **2008**, *4*, 435−447.
(67) Crescenzi, O.; Tomaselli, S.; Guerrini, R.; Salvadori, S.; D'Ursi, A. M.; Temussi, P. A.; Picone, D. Solution structure of the Alzheimer amyloid β-peptide (1−42) in an apolar microenvironment. *Eur. J. Biochem.* **2002**, *269*, 5642−5648.
(68) Berendsen, H. J. C.; Grigera, J. R.; Straatsma, T. P. The missing term in effective pair potentials. *J. Phys. Chem.* **1987**, *91*, 6269−6271.
(69) Bussi, G.; Donadio, D.; Parrinello, M. Canonical Sampling Through Velocity Rescaling. *J. Chem. Phys.* **2007**, *126*, No. 014101.
(70) Darden, T.; York, D.; Pedersen, L. Particle Mesh Ewald: An N·log(N) Method for Ewald Sums in Large Systems. *J. Chem. Phys.* **1993**, *98*, 10089−10092.
(71) Essmann, U.; Perera, L.; Berkowitz, M. L.; Darden, T.; Lee, H.; Pedersen, L. G. A Smooth Particle Mesh Ewald Method. *J. Chem. Phys.* **1995**, *103*, 8577−8593.
(72) Oostenbrink, C.; Villa, A.; Mark, A. E.; Van Gunsteren, W. F. A biomolecular force field based on the free enthalpy of hydration and solvation: The GROMOS force-field parameter sets 53A5 and 53A6. *J. Comput. Chem.* **2004**, *25*, 1656−1676.

https://doi.org/10.1021/acsphyschemau.3c00041
ACS Phys. Chem Au 2024, 4, 57−66

(73) Nosé, S. A Unified Formulation of the Constant Temperature Molecular Dynamics Methods. *J. Chem. Phys.* **1984**, *81*, 511−519.
(74) Hoover, W. G. Canonical Dynamics: Equilibrium Phase-space Distributions. *Phys. Rev. A* **1985**, *31*, 1695−1697.
(75) Kabsch, W.; Sander, C. Dictionary of protein secondary structure: Pattern recognition of hydrogen-bonded and geometrical features. *Biopolymers* **1983**, *22*, 2577−2637.
(76) Jiao, Y.; Yang, P. Mechanism of Copper(II) Inhibiting Alzheimer's Amyloid β-Peptide from Aggregation: A Molecular Dynamics Investigation. *J. Phys. Chem. B* **2007**, *111*, 7646−7655.
(77) Coskuner-Weber, O. Revisiting Cu(II) Bound Amyloid-β40 and Amyloid-β42 Peptides: Varying Coordination Chemistries. *J. Turkish Chem. Soc. Sect. Chem.* **2018**, *5*, 981−1008.
(78) La Penna, G.; Li, M. S. Towards High-Throughput Modelling of Copper Reactivity Induced by Structural Disorder in Amyloid Peptides. *Chem.—Eur. J.* **2018**, *24*, 5259−5270.
(79) Santis, D. E.; Minicozzi, V.; Proux, O.; Rossi, G.; Silva, K. I.; Lawless, M. J.; Stellato, F.; Saxena, S.; Morante, S. Cu(II)−Zn(II) Cross-Modulation in Amyloid−Beta Peptide Binding: An X-ray Absorption Spectroscopy Study. *J. Phys. Chem. B* **2015**, *119*, 15813−15820.
(80) Hansen, J.-P.; McDonald, I. R. *Theory of Simple Liquids, Third ed.*, 3rd ed.; Academic Press, 2006.
(81) Barroso da Silva, F. L. A.; Sterpone, F.; Derreumaux, P. OPEP6: A New Constant-pH Molecular Dynamics Simulation Scheme with OPEP Coarse-Grained Force Field. *J. Chem. Theory Comput.* **2019**, *15*, 3875−3888.

https://doi.org/10.1021/acsphyschemau.3c00041
ACS Phys. Chem Au 2024, 4, 57−66